Atomic structures and electronic properties of Ni or N modified Cu/diamond interface

Xue-Rong Shi[1,3] ⊙**, Simin Huang**[1]**, Yue Huang**[1]**, Yajing Zhang**[1]**,
Shibiao Zong**[1]**, Shusheng Xu**[1]**, Yanyan Chen**[2] **and Pan Ma**[1]

[1] School of Material Engineering, Shanghai University of Engineering Science, 333 Longteng Road,
Songjiang District, Shanghai, People's Republic of China
[2] State Key Laboratory of Coal Conversion, Institute of Coal Chemistry, Chinese Academy of Sciences,
27 South Taoyuan Road, Taiyuan, People's Republic of China

E-mail: shixuer05@mails.ucas.ac.cn

CrossMark

Abstract
The interfacial stability of copper/diamond directly affects its mechanical properties and thermal
conductivity. The atomic structures and electronic properties of Cu/diamond and Cu/X/diamond
interfaces have been identified to investigate the effect of interfacial additive X (X = Ni or N) on
the low-index interfacial adhesion of copper/diamond composites. For unmodified composites,
the interfacial stability decreases in the order of Cu(0 0 1)/diamond(0 0 1) > Cu(1 1 1)/
diamond(1 1 1) > Cu(0 1 1)/diamond(0 1 1). The metallic interfacial additive Ni is found to
enhance the Cu(0 1 1)/diamond(0 1 1) interfacial stability and exchange the interfacial stability
sequence of (0 1 1) and (1 1 1) composites. The nonmetallic element N will promote the stability
of Cu(1 1 1)/diamond(1 1 1) but not alter the stability order of the composites at different
interfaces. To explain the origin of interfacial stability, a series of analyses on atomic structures
and electronic properties have been carried out, including the identification of the type of formed
interfacial boundaries, the measurement of interfacial bond lengths, and the calculations of
density of states, bond populations, and atomic charge. The stability of the interface is found to
be related to the type of formed interfacial boundary and bond, the interfacial bond populations,
and the interfacial bond numbers. The layer-projected density of states reveals that all of the
considered interfaces exhibit metal characteristics. The interfacial Ni additive is found to be an
electron donor contributing the electrons to its bonded Cu and C atoms while the interfacial N
atom is an electron acceptor where it mainly accepts the electrons from its bonded Cu and C.

Keywords: copper/diamond, Ni interlayer, N interlayer, interfacial stability, first-principles
calculations

S Supplementary material for this article is available online

(Some figures may appear in colour only in the online journal)

1. Introduction

Driven by the rapid development of advanced miniaturization
of micro-electronic devices, copper/diamond composites gain
much attention as the electronics packaging materials due to
their extremely desirable electrical and mechanical properties
[1–4]. However, the poor wettability between diamond and
Cu resulting in the weak interfacial adhesion, which directly
affects the thermal conductivity and mechanical properties of
the composites such as fracture toughness and thermal expansion coefficient, limits its application [5, 6].

To improve interfacial wettability and strengthen the interfacial bonding, an effective way is to add the third elements
between Cu and diamond [7, 8]. Dong *et al* [6] found at 1400 °C,
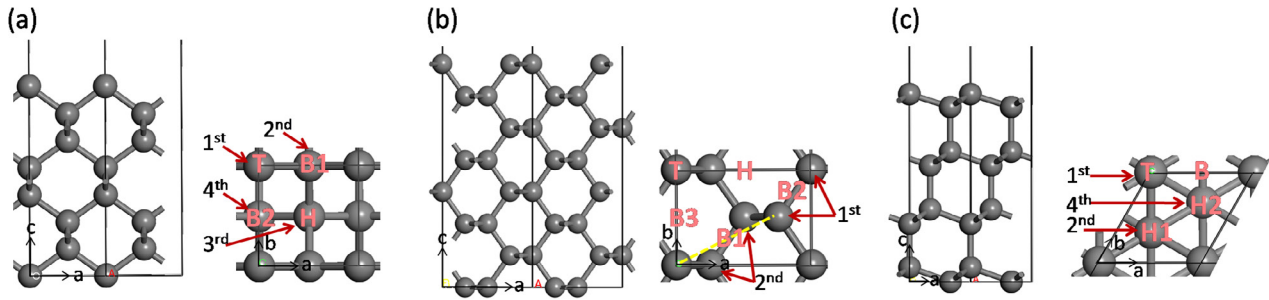
Figure 1. Side and top views of (a) diamond(0 0 1), (b) diamond(0 1 1), and (c) diamond(1 1 1) surfaces. The corresponding adsorption sites and carbon atoms at different layers are marked on the top view of the structure.

the contact angle between the liquid copper and diamond was as high as about 130° while after coating Ti on diamonds, it dropped to 25° between Ti-coated diamonds and copper. Using Auger electron spectroscopy, Zhang *et al* [9] and Lin *et al* [10] found that the coated Ti reacted with diamond to form TiC. Other experimental groups [1, 11–14] found the addition of Cr to copper/diamond composites could also improve the thermal conductivity and mechanical properties of materials by forming chromium carbide. Further first-principles calculations show that the Cr_3C_2(0 0 1)/diamond(0 0 1) interfacial bonding characteristic is a mixture of covalent and ionic bonds [15]. Additional to the metallic interfacial additive, previous studies have shown that the addition of nonmetallic elements into the interface of the copper/diamond composite can also change its mechanical properties. For example, previous experimental and theoretical works both found H or F was a promising passivation element in reducing the adhesion and improving tribological properties for Cu/diamond system [16–18]. In contrast, very thin boron interlayers have been found to improve the mechanical and thermal properties of Cu/diamond composites [19, 20].

In the present study, we chose two interfacial additive elements, metal Ni and nonmetal N to study the effect of interfacial additive on the adhesive behaviour of the Cu/diamond composites. They are chosen because (i) Metal Ni can potentially form CuNi alloy with Cu [21–23] and nickel carbide with C [24, 25]; (ii) N may form $CuCN_x$ ($X = 1, 2$) compound with C and Cu, [26, 27] and it may be suitable to match the phononic heat conduction of C because of its nearly the same mass with C. The use of Ni or N as a copper/diamond composite interfacial additive has not been found yet. In addition, previous studies concentrated on the effects of interfacial additive on the properties of a single low-index interface such as (0 0 1) [15] or (1 1 1) [17, 28] of composites, while systematical researches of the interfacial properties of three low-index interfaces have yet to be carried out.

Based on this, the interfacial properties (geometric and electronic) of copper/diamond composites with and without interfacial additive (Ni or N) were studied by first-principles calculations. Three interfaces, Cu(0 0 1)/diamond(0 0 1), Cu(0 1 1)/diamond(0 1 1), and Cu(1 1 1)/diamond(1 1 1), were considered comprehensively to find out the low-index interface with the best interfacial bonding performance. The effect of interfacial additive (metal Ni and nonmetal N) on the bonding performance of diamond/copper composites and the interfacial bond nature have been discussed.

2. Models and methods

Because of the hardness of diamond and the ductility of copper, the interfacial lattice constant is fixed to the lattice constant of diamond [5, 15, 16], while Cu is relaxed to match it. Three low-index interfaces, Cu(0 0 1)/diamond(0 0 1), Cu(0 1 1)/diamond(0 1 1), and Cu(1 1 1)/diamond(1 1 1), are built.

The diamond (0 0 1), (0 1 1), and (1 1 1) surfaces all have a thickness of eight carbon layers where the bottom C atoms are saturated by H atoms [29, 30]. The bottom four layers together with the saturating H atoms in diamond slabs were fixed to simulate bulk diamond. We considered four (one top T, two bridge B1 and B2, and one hollow H), five (one top T, three bridge B1–B3, and one hollow H), and four (one top T, one bridge B, and two hollow H1 and H2) adsorption sites for diamond (0 0 1), (0 1 1) and (1 1 1) surfaces, respectively.

The Cu(0 0 1), Cu (0 1 1), and Cu (1 1 1) slabs include five, seven, and four layer thicknesses [31, 32]. In which, we take one bottom corner atom of each slab as the aiming point to put on the adsorption site defined in figure 1 to construct the composite interface.

The density functional theory calculations with plane-wave ultra-soft pseudopotential approach [33] and the generalized gradient approximation of Perdew–Burke–Ernzerhof functional [34] is performed using the CASTEP code [35]. The cutoff energy is 400 eV. The K points of the bulk phase, (0 0 1), (0 1 1), and (1 1 1) surfaces are $8 \times 8 \times 8$, $6 \times 6 \times 1$, $4 \times 6 \times 1$, and $7 \times 7 \times 1$ respectively. Spin polarization is considered for systems containing unpaired electrons. The force convergence criterion is 0.01 eV Å^{-1}. All the parameters including the layer thickness are tested with change of the work of adhesion of the Cu/diamond interface smaller than 4% (table S1 (stacks.iop.org/JPhysCM/32/225001/mmedia) in SI).

To describe the interfacial binding strength quantitatively, the ideal work of adhesion of the Cu/diamond interface is defined by [15, 36]

$$W_{ad} = \frac{E_{Cu} + E_{diamond} - E_{tot}}{A}. \quad (1)$$

E_{tot}, E_{Cu}, and $E_{diamond}$ are the total energies of the optimized Cu/diamond interface, a single diamond surface, and a single copper surface, respectively. A is the interfacial area. The larger the work of adhesion, the stronger the interfacial binding of the copper/diamond composites.
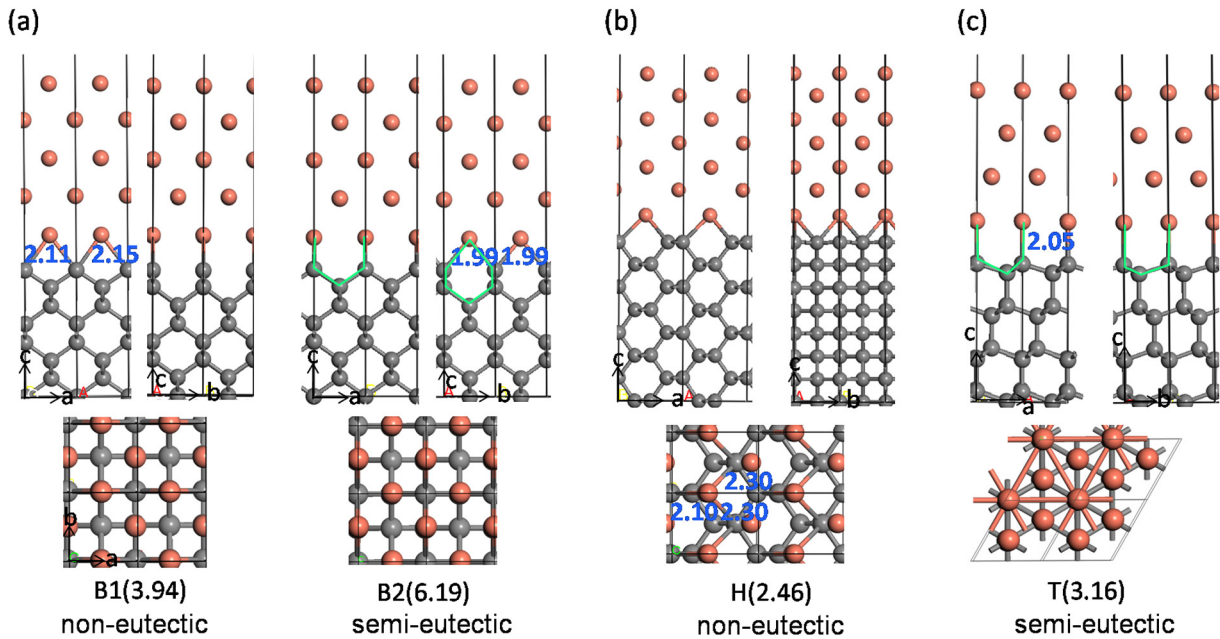
Figure 2. Side (top row) and top (bottom row) views of Cu/diamond interfacial structures. The corresponding W_{ad} (J/m^2) is provided at the bottom and bond distances between C and its bonded Cu d(C–Cu) (Å) are labelled. To make the figure clear, the bottom saturating H atoms are hidden and only the bonds in diamond and at the interface are shown by sticks. The green lines connecting the atoms are the hint lines to recognize the interfacial boundary type. C and Cu are presented by the gray and brick spheres, respectively.

Note that the addition of Ni or N interlayer between Cu and diamond will create two interfaces, the interface between Cu and X-diamond (denoted by Interf.I) and the interface between Cu–X and diamond (denoted by Interf.II). For Interf.I, the interfacial work of adhesion is calculated by

$$W_{ad} = \frac{E_{Cu} + E_{X\text{-}diamond} - E'_{tot}}{A} \quad (2)$$

where E'_{tot} and $E_{X\text{-}diamond}$ are the total energies of the optimized Cu/X/diamond composites and the diamond surface with the adsorbed additive X (X = Ni or N). For Interf.II, the corresponding interfacial work of adhesion is defined by

$$W_{ad} = \frac{E_{Cu\text{-}X} + E_{diamond} - E'_{tot}}{A}. \quad (3)$$

Here $E_{Cu\text{-}X}$ is the total energy of the optimized Cu surface with the adsorbed additive X (X = Ni or N) at the Cu lattice parameter.

3. Results and discussion

3.1. Cu/diamond interface

For Cu(0 0 1)/diamond(0 0 1), four initial structures yield two stable interfacial structures B1 with the shortest interfacial C–Cu bond distance of 1.99 Å and B2 with the shortest interfacial C–Cu bond distance of 2.11 Å where initial T and H convert to B2 (table 1). The corresponding work of adhesion for B1 and B2 is 3.94 and 6.19 J m^{-2}, respectively, suggesting that the energetically preferable Cu(0 0 1)/diamond(0 0 1) interfacial structure is B2. The stronger stability of B2 may result from the formation of semi-eutectic interfacial boundary by Cu(0 0 1) and diamond(0 0 1). As shown in figure 2, the interfacial Cu from Cu side fits into the diamond lattice (see the

Table 1. The work of adhesion W_{ad} (J/m^2) and shortest interfacial bond distance between C and Cu d(C–Cu) (Å) of diamond/Cu.

Diamond/Cu	site	W_{ad}	d(C–Cu)
(0 0 1)/(0 0 1)	T, H	→B2	—
	B1	3.94	2.11
	B2	6.19	1.99
(0 1 1)/(0 1 1)	T, B1–B3	→H	—
	H	2.46	2.10
(1 1 1)/(1 1 1)	T	3.16	2.05
	B, H, T	→T	—

atoms connected by the green line) forming the semi-eutectic boundary. While for B1 structure, neither the interfacial Cu from Cu side nor the interfacial carbon from diamond side can emerge into the lattice of the other side resulting into the non-eutectic boundary.

For Cu(0 1 1)/diamond(0 1 1), five initial interfacial structures result in one stable interfacial configuration yielding W_{ad} of 2.46 J m^{-2} and the shortest C–Cu bond length of 2.10 Å. The Cu(0 1 1)/diamond(0 1 1) forms a non-eutectic boundary.

For the Cu(1 1 1)/diamond(1 1 1) interface, only one stable interfacial structure is obtained from four initial structures. The obtained T structure yields the work of adhesion W_{ad} of 3.16 J m^{-2}, and the corresponding C–Cu bond length of the interface is 2.05 Å. Similar to B2 of Cu(0 0 1)/diamond(0 0 1), the Cu(1 1 1)/diamond(1 1 1) interface forms a semi-eutectic boundary.

Summarizing, among three low-index interfaces, the Cu(0 0 1)/diamond(0 0 1) interface is the most stable with the work of adhesion W_{ad} larger than 3.94 J m^{-2}, followed by Cu(1 1 1)/diamond(1 1 1) with W_{ad} of 3.16 J m^{-2}. The Cu(0 1 1)/diamond(0 1 1) is the least stable with W_{ad} of only 2.46 J m^{-2}.

Table 2. The relative energy ΔE (eV) and corresponding C–Ni (C–N) bond length (Å) for Ni and N adsorption on low-index surface of diamond.

	Site	ΔE_{Ni}[a]	d(C–Ni)	ΔE_{N}[a]	d(C–N)
(0 0 1)	T	+0.63	1.79	+1.06	1.26
	B2	0.00	1.90/1.90	0.00	1.50/1.50
(0 1 1)	T	—	—	+1.08	1.43
	B1	+0.02	1.99/1.99	0.00	1.37/1.37
	B2	—	—	+1.56	1.43/1.43
	B3	+0.63	1.89/2.09/2.09	—	—
	H	0.00	1.97/2.15/2.16	—	—
(1 1 1)	T	+0.00	1.94	0.00	1.42
	B	—	—	+2.09	1.42/1.52

[a] The energy difference refers to the most stable sates on each surface. More positive, less stable.
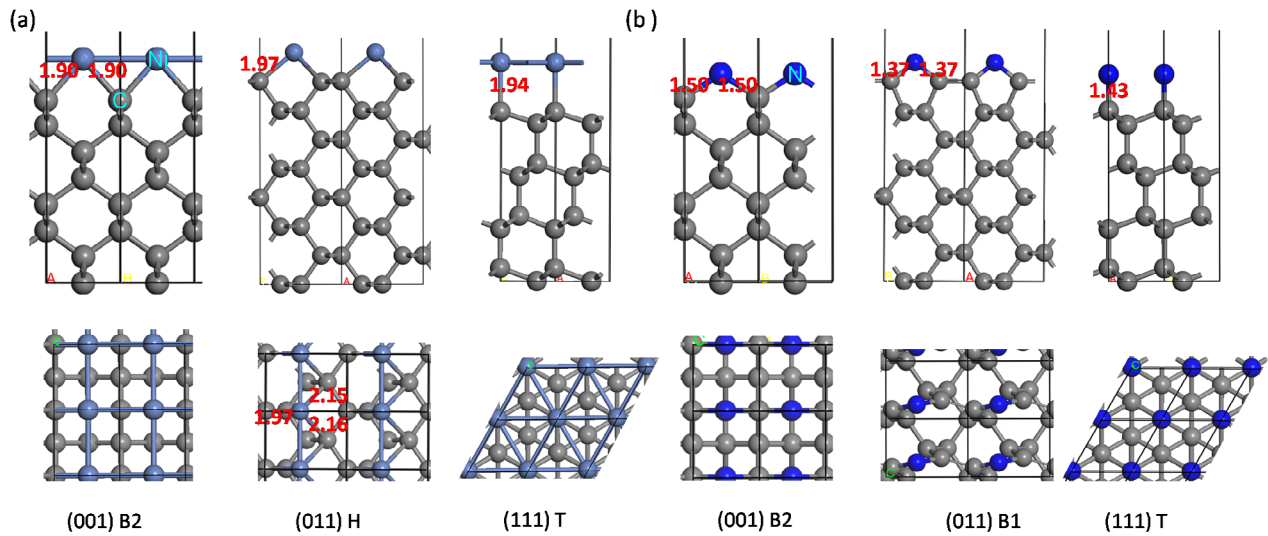
Figure 3. Side (top row) and top (bottom row) views of the most stable configuration for (a) Ni and (b) N adsorption on each low-index diamond surface. The formed Ni–C and N–C bond lengths (Å) are labeled. The bottom saturating H atoms are hidden. C, N, and Ni are shown by the gray, dark blue, and blue spheres, respectively.

3.2. Adsorption of additive atoms on diamond

Of the thirteen different adsorption sites at the diamond surfaces (see figure 1), only six sites, T and B2 at diamond(0 0 1), B1, B3 and H at diamond(0 1 1), and T at diamond(1 1 1), yield stable Ni adsorption (figures 3(a) and S1). Ni approaching near the B1 and H at diamond(0 0 1), B2 and T at diamond(0 1 1), and B, H1, and H2 at diamond(1 1 1) leads to adsorption at T and B2 at diamond(0 0 1), H at diamond(0 1 1), T at diamond(1 1 1), respectively.

Among two obtained structures for atomic Ni adsorption on diamond(0 0 1), the B2 structure is more stable than the T structure with the energy of 0.63 eV lower. For Ni adsorption on diamond(0 1 1), the H and B1 structures are close in stability with the energy difference between each other is only 0.02 eV and B3 is less stable than them with about 0.63 eV higher in energy. For Ni adsorption on diamond(1 1 1), only one stable configuration T is obtained (table 2).

For N adsorption on diamond surfaces, thirteen initial structures yield seven stable local minima. N approaching to B1 and H at (0 0 1), B3 and H at (0 1 1), and H1 and H2 at (1 1 1) results in the adsorption at T and B2 on (0 0 1), B1 on (0 1 1), and T on (1 1 1), respectively.

For N adsorption on diamond(0 0 1), B2 is more stable than T structure with the energy difference of 1.06 eV. On diamond (0 1 1), the stability of three structures decreased in the sequence of B1 > T > B2 where B2 is 1.56 eV higher in energy than B1. On diamond(1 1 1), the T structure is much more stable than B by 2.09 eV lower in energy. In addition, it was found that the formed C–N bond length of the different surfaces is approximately in the range of 1.26 to 1.52 Å, which is shorter than the formed C–Ni bond length ranging from 1.79 to 2.16 Å.

3.3. Cu/X/diamond interface

The most stable diamond (0 0 1), (0 1 1), and (1 1 1) structures with the adsorbed X (X = Ni or N) in figure 3 were used to construct the Cu/X/diamond composites. The X-diamond
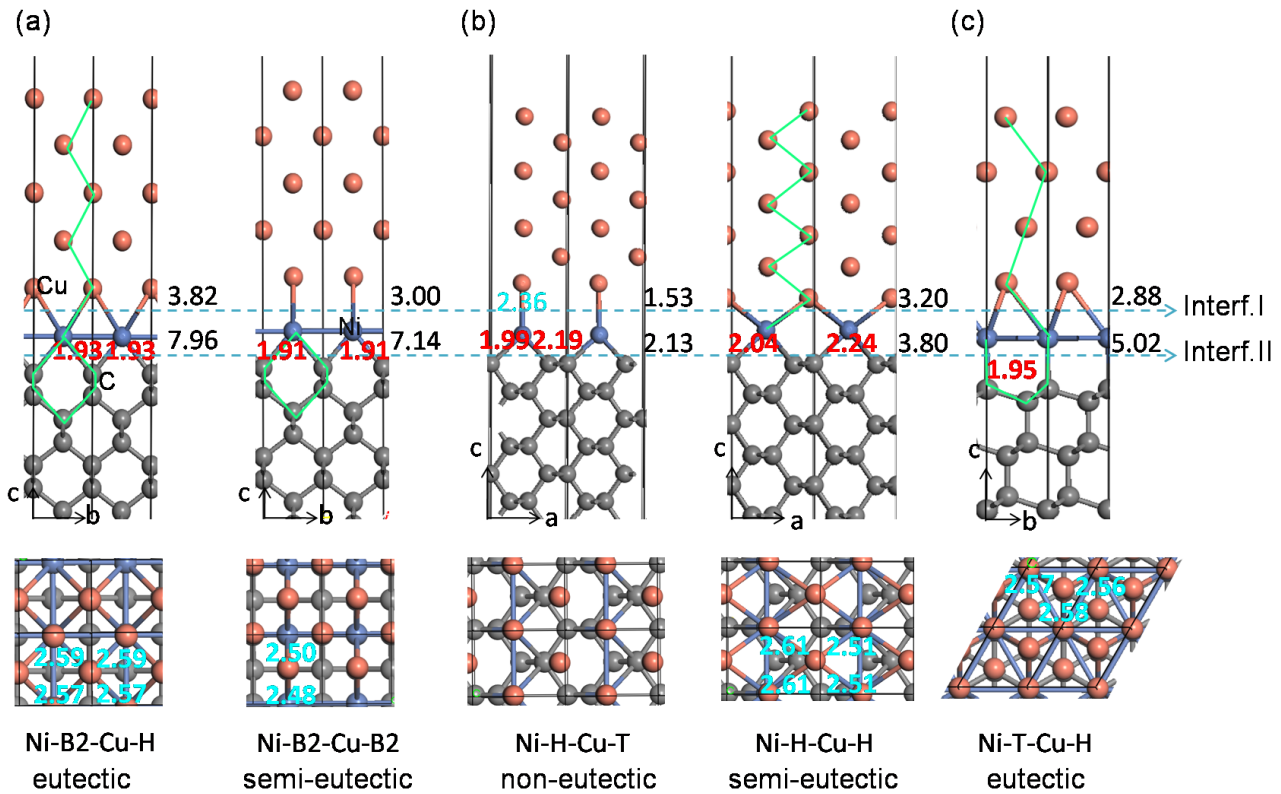
Figure 4. Side (top row) and top (bottom row) views of the interfacial structures of (a) Cu(0 0 1)/Ni/diamond(0 0 1), (b) Cu(0 1 1)/Ni/diamond(0 1 1), and (c) Cu(1 1 1)/Ni/diamond(1 1 1). W_{ad} (J/m^2) for Interf.I and Interf.II are provided on the blue dashed line in black. The C–Ni and Ni–Cu bond distances (Å) are labelled in red and cyan, respectively. The green lines connecting the stacking atom in the lattice are the hint lines for the recognition of the interfacial boundary type.

surfaces create new adsorption sites for copper slab to form the interfacial configurations by the additive element X. For the X-diamond (0 0 1), (0 1 1), and (1 1 1) surfaces, we considered four (one top X, two bridge X–X, and one hollow 4X), four (one top X, two bridge X–X, and one hollow 4X), and three (one top X, one bridge X–X, and one hollow 3X) sites, respectively.

For Cu(0 0 1)/Ni/diamond(0 0 1), four initial structures yield two stable interfacial structures H (denoted by Ni–B2–Cu–H in figure 4(a)) and B2 (denoted by Ni–B2–Cu–B2 in figure 4(a)) where initial T and B1 convert to H. The H interfacial structure is more stable than the B2 one with the work of adhesion of 3.82 and 7.96 J m^{-2} for Interf.I between Cu and X-diamond and Interf.II between Cu–X and diamond, which is 0.82 larger than that of B2, respectively. Here for the calculation of W_{ad} of Interf.II, the reference state for B2, namely, the top adsorption of Ni on Cu, results in the hollow site, which is the same to the reference state for T. Interestingly, the interfacial Ni in H can be embedded into the Cu and diamond lattice at the same time (see the green hint lines in figure 4(a)) yielding the eutectic boundary while in B2, Ni can only take the lattice point spot of diamond creating a semi-eutectic boundary. Hence, the H interface with the eutectic boundary is more stable than the B2 structure with the semi-eutectic boundary.

Of four initial configurations for Cu(0 1 1)/Ni/diamond(0 1 1), both B1 and B2 structures lead to the H structure (denoted by Ni–H–Cu–H in figure 4(b)). In H structure, Cu slab adsorption on the hollow site formed by four interfacial

Ni atoms gives the work of adhesion of 3.20 and 3.80 J m^{-2} for Interf.I and II, respectively, with the Cu–Ni bond length of 2.51, 2.51, 2.61, and 2.61 Å. The T structure with Cu slab adsorption on the top site of Ni (denoted by Ni–H–Cu–T in figure 4(b)) is less stable than H by 0.67 J m^{-2} smaller in W_{ad}. It is found that H forms a semi-eutectic boundary where interfacial Ni joins the Cu lattice while the T structure exhibits a non-eutectic boundary.

Among three initial structures of Cu(1 1 1)/Ni/diamond(1 1 1), only one stable interfacial structure H is obtained. In H, Cu slab adsorption on the hollow site formed by three interfacial Ni atoms gives the work of adhesion of 2.88 and 5.02 J m^{-2} for Interf.I and II, respectively. For Cu(1 1 1), its atoms exhibit a ABC packing along [1 1 1] direction (*c* axis in figure 4) where the interfacial Ni just occupied the position of copper B (assuming the toppest Cu at A site) meanwhile Ni also fits into the diamond lattice suggesting the formation of an eutectic boundary.

For the Cu/N/diamond composites, two, two, and two local energetically minima were obtained for Cu(0 0 1)/N/diamond(0 0 1), Cu(0 1 1)/N/diamond(0 1 1), and Cu(1 1 1)/N/diamond(1 1 1), respectively. The B2 structure with the Cu(0 0 1) adsorption on the neighbouring N (denoted by N–B2–Cu–B2 in figure 5(a)) gives W_{ad} of 3.27 and 14.14 J m^{-2} for Interf.I and Interf.II, respectively. The adsorption of Cu on the top of interfacial additive N is less stable by W_{ad} of 0.27 (3.49) J m^{-2} smaller for Interf.I (Interf.II). Both T and B2 structures for Cu(0 0 1)/N/diamond(0 0 1) exhibit semi-eutectic boundaries
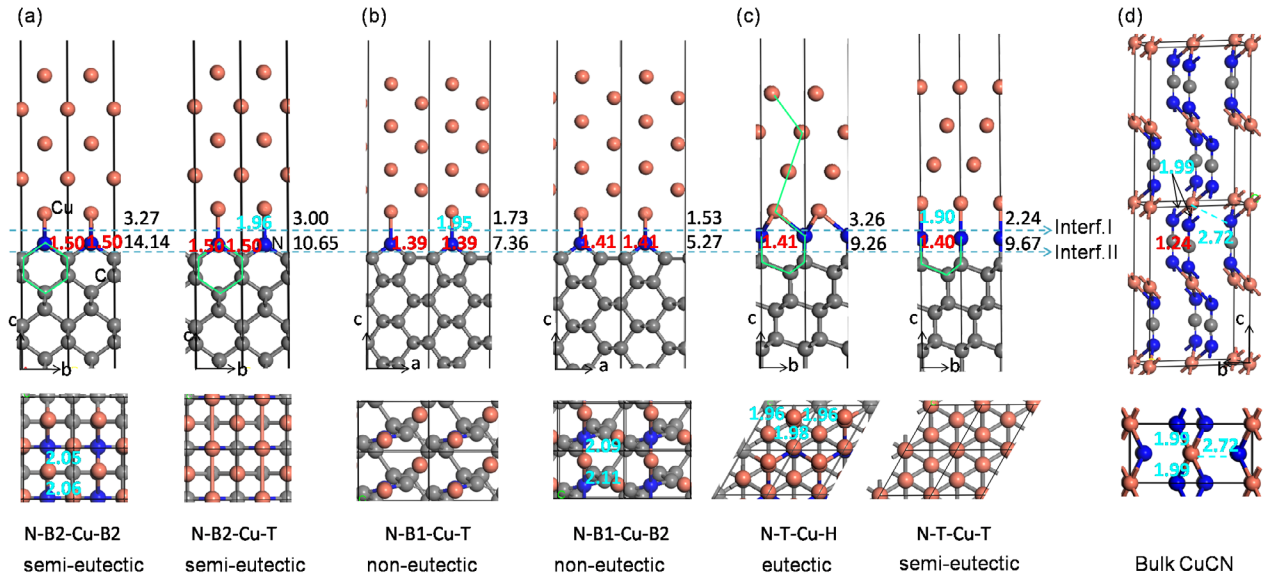
Figure 5. Side (top row) and top (bottom row) views of the interfacial structures of (a) Cu(0 0 1)/N/diamond(0 0 1), (b) Cu(0 1 1)/N/diamond(0 1 1), (c) Cu(1 1 1)/N/diamond(1 1 1), and (d) optimized bulk CuCN. W_{ad} (J/m^2) for Interf.I and Interf.II and interfacial C–N and N–Cu bond distances (Å) are labelled in black, red and cyan, respectively. The green lines connecting the atom in the lattice are the hint lines for the recognition of the interfacial boundary type.

where interfacial N is embedded in the diamond lattice with C-N bond length of 1.50 Å. Similar to Cu(0 0 1)/N/diamond(0 0 1), one top T and one bridged B2 interfacial structure at Cu(0 1 1)/N/diamond(0 1 1) were obtained. However, they both yield non-eutectic boundaries with W_{ad} of 1.73 (7.36) and 1.53 (5.27) J m^{-2} for Interf.I (Interf.II), respectively. For Cu(1 1 1)/N/diamond(1 1 1), an eutectic interfacial boundary is found in the H configuration. It gives W_{ad} of 3.26 and 9.26 J m^{-2} for Interf.I and II, respectively. The T structure with a semi-eutectic interfacial boundary exhibits smaller W_{ad} by 1.12 J m^{-2} for Interf.I but larger W_{ad} by 0.41 J m^{-2} for Interf.II. The reversal stability for Interf.II between H and T results from the less stable of reference state of Cu–N for T where N top adsorption on Cu is 0.77 eV higher in energy than its fcc hollow (reference state of Cu–N for H) adsorption. While the Cu(1 1 1)/N/diamond(1 1 1) with N–T–Cu–H is more stable than the N–T–Cu–H structure by 0.35 eV lower in energy. Namely, the total energy difference for Cu(1 1 1)/N/diamond(1 1 1) between H and T cannot compensate the total energy difference between two reference states between Cu–N(top) and Cu–N(fcc). Compared with the bulk CuCN structure (figure 5(d)), it is observed that among all the N modified interfaces, only the N–T–Cu–H configuration at Cu(1 1 1)/N/diamond(1 1 1)interface forms a quasi-bulk-CuCN structure where N is on the top of C and Cu is on the hollow site of N.

Summarizing, on the same surface, the structure with an eutectic interfacial boundary is more stable than that with a semi-eutectic interfacial boundary (see Cu(0 0 1)/Ni/diamond(0 0 1) and Cu(1 1 1)/N/diamond(1 1 1)) and the one with a semi-eutectic interfacial boundary is more stable than that with a non-eutectic interfacial boundary (Cu(0 1 1)/Ni/diamond(0 1 1)). Metallic interfacial additive Ni is found to enhance the Cu(0 1 1)/diamond(0 1 1) interfacial stability and the nonmetallic element N will promote the stability of

Table 3. The work of adhesion W_{ad} (J/m^2) for the most stable interfacial structure.

|	Cu/diamond	Cu/Ni/ diamond	Cu/N/ diamond
(0 0 1)/(0 0 1)	6.19 (2)[c]	3.82[a] (3)[c]	3.27[a] (2)[c]
		7.96[b] (2)[c]	14.14[b] (2)[c]
(0 1 1)/(0 1 1)	2.46 (3)[c]	3.20[a] (4)[c]	1.73[a] (1)[c]
		3.80[b] (3)[c]	7.36[b] (2)[c]
(1 1 1)/(1 1 1)	3.16 (1)[c]	2.88[a] (3)[c]	3.26[a] (3)[c]
		5.02[b] (1)[c]	9.26[b] (1)[c]

[a] For Interf.I between Cu and X-diamond.
[b] For Interf.II between Cu-X and diamond.
[c] Number of interfacial bonds.

Cu(1 1 1)/diamond(1 1 1) (table 3). The adhesion of Interf.II is found to be always stronger than copper/diamond, and combined with the number of formed interfacial bonds, we can conclude that the bond strength decreases in the order of C–N > C–Ni > C–Cu.

3.4. Electronic properties

3.4.1. Density of states. The interfacial stability are controlled by many factors [37–39], and to gain the relationship between the electronic structure and interfacial stability, the total and layer projected partial density of states (TDOS and LPDOS) of separated Cu and diamond slab, Cu/diamond, Cu/Ni/diamond, and Cu/N/diamond systems are provided in figures 6, 7 and S2 in SI. The calculated TDOSs show that the electronic states at E_f appear at all cases, indicating that the interfaces show a metallic character. Similar results have been found for the pure diamond surfaces and Cr$_3$C$_2$/diamond system [15, 40, 41]. Interestingly, we observed that TDOSs near the Fermi level for the more stable interfacial structures,
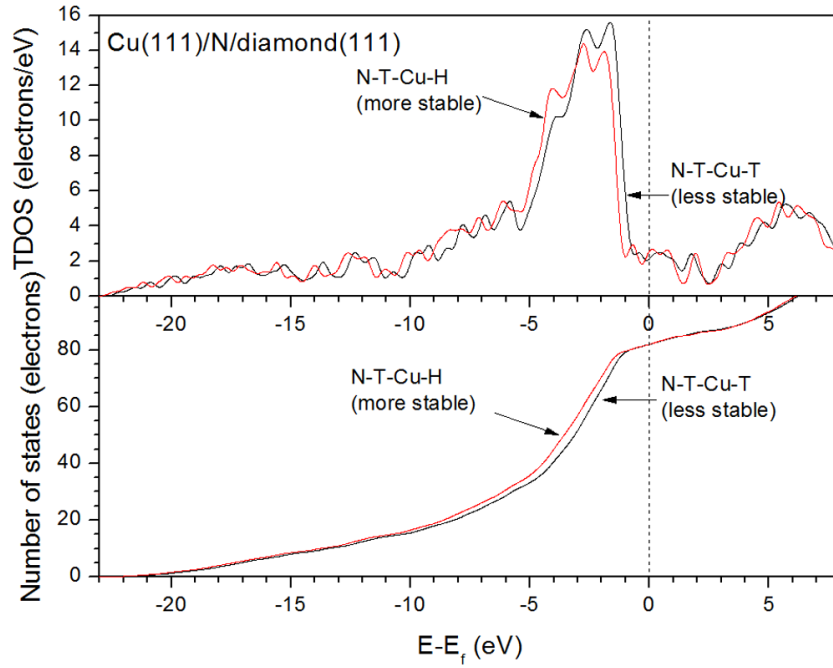
Figure 6. The total (up) and integrated (down) density of states for two configurations of Cu(1 1 1)/N/diamond(1 1 1).
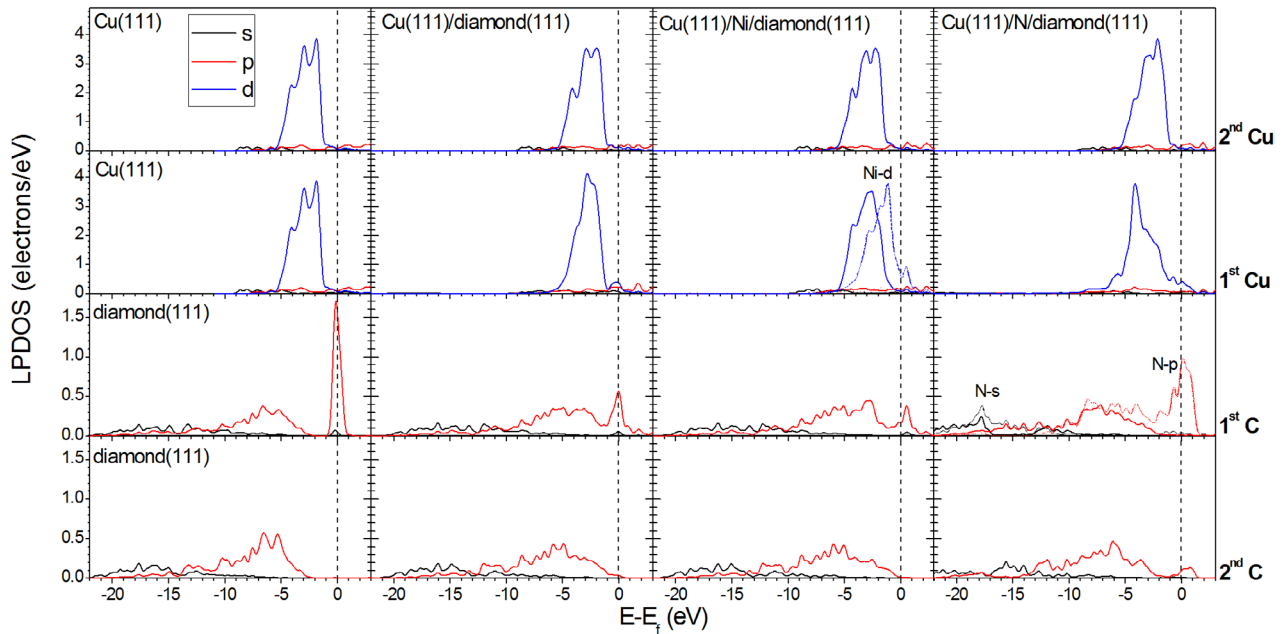

Figure 7. The LPDOS for (1 1 1) systems. The interface is between the first Cu and first C layers.

such as N–T–Cu–H at Cu(1 1 1)/N/diamond(1 1 1), decreased compared with the less stable one, N–T–Cu–T at Cu(1 1 1)/N/diamond(1 1 1) (figure 6), leading to more electrons occupying the lower states and a smoother TDOS curve near E_f.

According to LPDOSs (figure 7), the major contribution to the density of the interface states near E_f is from C/N 2p and its bonded Cu/Ni 3d orbitals. For Cu(1 1 1)/diamond(1 1 1), 1st C 2p make the most contribution to the electron states at E_f. For Cu/Ni/diamond, the density of the interface states near E_f is mainly from the interfacial additive Ni 3d and the 1st layer of C 2p orbitals at the Cu/Ni/diamond interface. For Cu/N/diamond, most of the density of the interface states near E_f comes from the interfacial additive N 2p. Namely, before modification, the 1st layer of C atoms at the interface plays a major role to contribute to the density of the interface states at E_f, while after modification, the interfacial additive, Ni or N, becomes the major part inducing the decreased electronic density of its bonded 1st layer of C atoms at E_f. It is also noticed that compared with metallic additive Ni, nonmetallic additive N yields a stronger effect on the charge redistribution among the (1 1 1) composites series. It not only affects the relocation of the electronic states of its bonded 1st layer C and Cu, but also influences the nonbonded 2nd layer C and Cu atoms while Ni barely affects the electronic states distribution of the 2nd
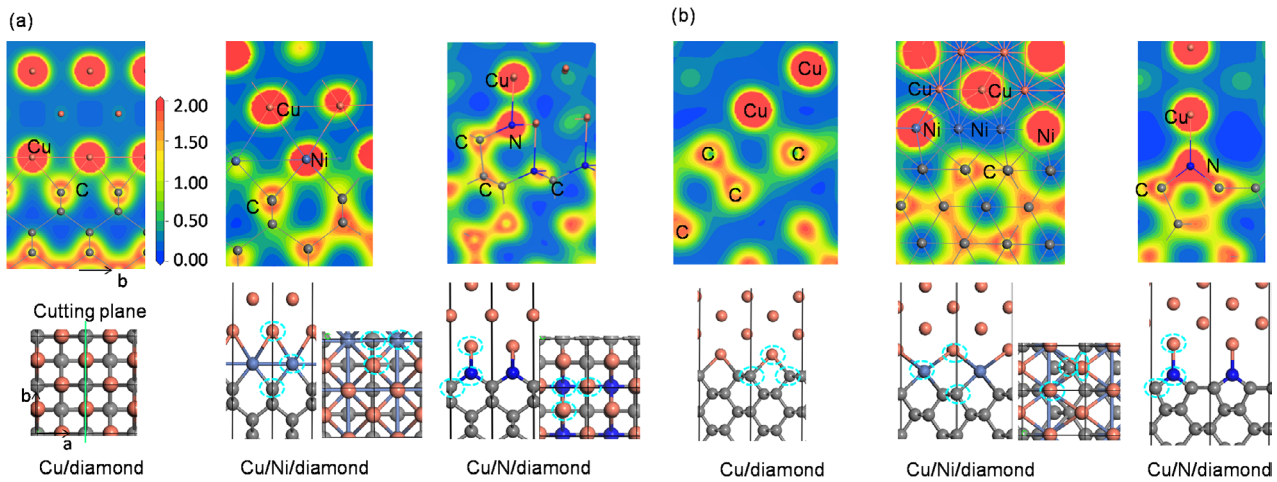
Figure 8. Charge density (e/Å³) (top row) and cutting plane (bottom row) for (a) (0 0 1) and (b) (0 1 1) composites. The cutting plane is the best-fit plane of three chosen atoms (marked by dashed circles).
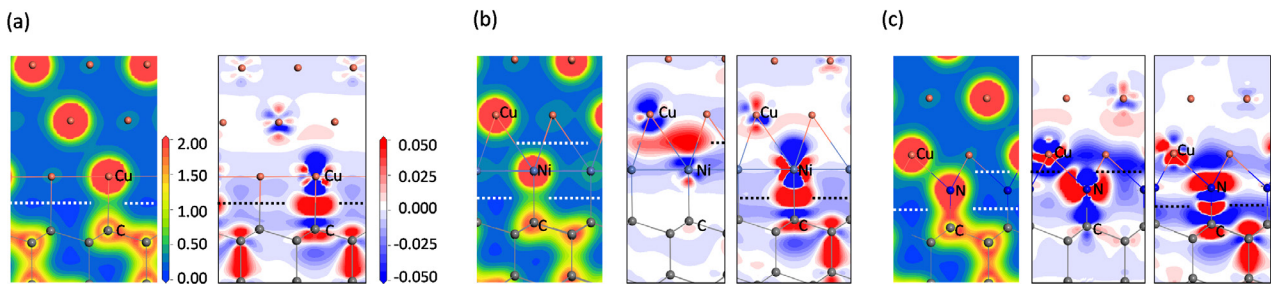
Figure 9. Charge density (left) and charge density difference (right) maps for (1 1 1) composites. The location of the interface is indicated by dotted lines. The charge density difference refers to the changes in the electron distribution before and after the formation of interfacial bonds. The color difference represents the total and change of the electron density (e/Å³) for charge density and charge density difference maps, respectively. The cutting plane is along T-H1 in figure 1.

layer C and Cu orbitals. Compared with the isolated Cu(1 1 1) surface, the 1st Cu 4s peaks in composites redistribute in the range of −9 eV to −4 eV indicating that 1st Cu 4s participates in the interfacial bonding. An obvious overlap between the C 2p orbital at the 1st layer of diamond (1 1 1) and Cu 3d orbitals at the 1st layer or interfacial additive Ni 3d in the range of −5 eV to 0 eV was found suggesting the strong hybridization between the interfacial C 2p states and Cu 3d or Ni 3d orbitals. Furthermore, a significant d–d orbitals hybridization between interfacial Cu 3d and Ni 3d states ranging from −5 eV to 0 eV for Cu(1 1 1)/Ni/diamond(1 1 1) was revealed. For Cu(1 1 1)/N/diamond(1 1 1), there is a strong p–p (s–s) orbitals hybridization between the interfacial C and additive N in the range of −19(−25) eV to 0 (−10) eV with the resonant peak at about −8(−18) eV. It reveals the formation of strong C–N covalent bonds, which is further confirmed by the following charge density and charge density difference analyses.

3.4.2. Charge density and charge density difference maps. As observed from the charge density map in figures 8 and 9, for Cu/diamond, the charge distributions of Cu atoms are nearly spherically symmetric while those of C atoms show a polarization toward Cu suggesting the formation of C–Cu ionic bonds. The similar character of C–Ni ionic bonds was observed for Cu/Ni/diamond while the bonded Cu and Ni form metallic bonds due to the nearly spherically symmetric charge

distributions around them. For Cu/N/diamond, the charge distributions of the interfacial Cu atoms also exhibit the nearly spherically symmetric feature suggesting the formation of N–Cu ionic bonding at the interfaces again while the charge distributions of bonded N and C atoms at the interface show a distortion directing toward each other suggesting the formation of strong C–N covalent bonds. Meanwhile, the electron charges around C have been found more approaching to the N atoms other than to the Cu atoms and a stronger charge accumulation between the interfacial C atoms and N atoms than that between the bonded C and Cu has been observed revealing that C–N covalent bonds are stronger than C–Cu ionic bonds. This is consistent with the corresponding work of adhesion of interface, for all cases, the W_{ad} between Cu–N and diamond is larger than that between Cu and N-diamond indicating Interf.II is more stable than Interf.I.

3.4.3. Mulliken atomic populations. As shown in table 4, for Cu/diamond composites, the electrons transfer from the 4p and 3d orbitals of Cu to 2s and 2p orbitals of its bonded C atoms. The electron number decreases from 0.78 and 9.72 of bulk Cu to 0.49–0.60 and 9.62–9.66 in composites for the 4p and 3d orbitals of 1st Cu, respectively. Meanwhile, the electron number around 2s and 2p of the bonded 1st C increases from 1.10 and 2.90 to 1.20–1.30 and 2.95–3.01. For Cu/Ni/diamond, the interfacial Ni atom denotes the electron to the

Table 4. Mulliken atomic charges (|*e*|) and bond populations.

System	Atom[a]	s	p	d	Total	Charge	Bond population
All slab	Bulk Cu	0.50	0.78	9.72	11.00	0	—
	Bulk C	1.10	2.90	0	4.00	0	—
(0 0 1)/(0 0 1)	1st Cu	0.53	0.60	9.62	10.75	0.25	0.66
	1st C	1.30	2.96	0	4.26	−0.26	(Cu–C)
(0 1 1)/(0 1 1)	1st Cu	0.55	0.49	9.64	10.69	0.31	0.03
	1st C	1.20	2.98	0	4.18	−0.18	0.05
		1.20	3.01	0	4.20	−0.20	(Cu–C)
(1 1 1)/(1 1 1)	1st Cu	0.62	0.58	9.66	10.87	0.13	0.10
	1st C	1.20	2.95	0	4.15	−0.15	(Cu–C)
(0 0 1)/Ni/(0 0 1)	1st Cu	0.57	0.78	9.71	11.06	−0.06	−0.12 (Cu–Ni)
	Ni	0.42	0.55	8.67	9.64	0.36	0.63
	1st C	1.30	2.97	0	4.26	−0.26	(Ni–C)
(0 1 1)/Ni/(0 1 1)	1st Cu	0.60	0.78	9.71	11.10	−0.10	0.28 (Cu–Ni)
	Ni	0.42	0.41	8.70	9.52	0.48	0.10
	1st C	1.21	2.97	0	4.18	−0.18	0.19
		1.21	3.01	0	4.21	−0.21	(Ni–C)
(1 1 1)/Ni/(1 1 1)	1st Cu	0.55	0.77	9.71	11.03	−0.03	−0.44 (Cu–Ni)
	Ni	0.51	0.60	8.69	9.80	0.20	0.05
	1st C	1.20	2.93	0	4.14	−0.14	(Ni–C)
(0 0 1)/N(0 0 1)	1st Cu	0.50	0.59	9.67	10.76	0.24	0.46 (Cu–N)
	N	1.57	3.88	0	5.45	−0.45	1.50
	1st C	1.12	2.72	0	3.84	0.16	(N–C)
(0 1 1)/N/(0 1 1)	1st Cu	0.62	0.45	9.71	10.78	0.22	0.34 (Cu–N)
	N	1.53	3.86	0	5.39	−0.39	0.81
	1st C	1.09	2.84	0	3.93	0.07	0.82
		1.09	2.84	0	3.93	0.07	(N–C)
(1 1 1)/N(1 1 1)	1st Cu	0.42	0.67	9.58	10.67	0.33	0.81 (Cu–N)
	N	1.64	3.82	0	5.46	−0.46	0.73
	1st C	1.11	2.83	0	3.94	0.06	(N–C)

[a] The interface is between the first Cu and first C layers.

bonded Cu and C atoms, specifically, devotes to the 4s orbital of Cu and 2s and 2p orbitals of the bonded C atoms. The charge of 4s orbital increases from 0.5 e of bulk to around 0.55 e in the doping case, and the charges of 4p and 3d orbitals of 1st Cu are nearly identical in the bulk Cu and composites. Similar to the Cu/diamond case, the charge of 2s and 2p orbitals of the bonded C atoms increases from the 1.10 e and 2.90 e in the bulk to 1.20–1.30 and 2.93–3.01 e. In contrast, interfacial N atoms mainly accept the electrons from 2p orbitals of its bonded Cu and C where the charge of 2p orbital of Cu decreases from 0.78 e of bulk to 0.45–0.67 e of composites while the trend of 4s orbital of 1st Cu depends on the interfaces. Compared with the bulk case, the 4s of 1st Cu charge keeps the same, increases and decreases for the (0 0 1), (0 1 1) and (1 1 1) composites, respectively. For the 1st C at the interface in Cu/N/diamond, the charge of 4s orbitals barely change while the 2p ortibals devotes the electrons yielding an decreased electron number of 2.72–2.84 e in composites from 2.90 e in bulk.

Summarizing, for Cu/diamond composites, the electrons transfer from the 4p and 3d orbitals of Cu to 2s and 2p orbitals of its bonded C atoms; for Cu/Ni/diamond, the interfacial Ni plays as the electron donor where the electrons are devoted to 4s orbital of its bonded Cu and 2s and 2p orbitals of its bonded

C atoms at the same time; for Cu/N/diamond, interfacial N atom is an electron acceptor where it mainly accepts the electrons from 2p orbitals of its bonded Cu and C.

To understand the bond elongation and contraction at the interface better, the bond population studies were performed. As shown in table 4 the bond population within the interfacial Cu–C bonds at Cu(0 0 1)/diamond(0 0 1) is the largest with 0.66, followed by that at the Cu(1 1 1)/diamond(1 1 1) with 0.10, and the Cu(0 1 1)/diamond(0 1 1) is smallest with about 0.05, which is consistent with the interfacial stability sequence. The shorter the interfacial bond length, the larger the bond population within the interfacial bond, and the more stable the interface structure is.

For Cu/Ni/diamond, among three composites, only Cu(0 1 1)/Ni/diamond(0 1 1) interface (both Interf.I and II) yields a larger bond population within the interfacial Cu–Ni and Ni–C than that within the unmodified interfacial Cu–C which is consistent with the interfacial stability. The work of adhesion W_{ad} calculations show that only the interfacial stability (both Interf.I and II) of Cu(0 1 1)/Ni/diamond(0 1 1) are enhanced by Ni among three composites.

For Cu/N/diamond, compared with the case of the unmodified interfacial Cu–C, the bond populations within the interfacial Cu–N becomes smaller, larger, and larger for the (0 0 1),

(0 1 1) and (1 1 1) composites, respectively, which is consistent with change of the interfacial bond lengths. The (0 0 1), (0 1 1) and (1 1 1) interfacial Cu–N bond lengths are 0.06 shorter, 0.15 longer, and 0.07–0.09 Å longer than the corresponding Cu–C bond distances. Note that the bond populations within the interfacial Cu–N is larger than those within the original Cu–C at Cu(0 1 1)/N/diamond(0 1 1) and composites, however, the work of adhesion W_{ad} shows the interfacial stability of Cu(0 1 1)/N/diamond(0 1 1) is weaker than Cu(0 1 1)/N/diamond(0 1 1). That is partially due to the reduced interfacial bond number where it decreases from three interfacial Cu–C bonds to one Cu–N bond.

4. Conclusions

The thermal conductivity and mechanical properties of copper/diamond are closely related to its interfacial stability. In this work, we employ first-principles calculations to investigate the interfacial structures and stabilities of Cu/diamond and Cu/X/diamond (X = Ni or N) combined at three low-index (0 0 1), (0 1 1), and (1 1 1) interfaces systematically.

The calculations show that the Cu/diamond interface stability decreases in the order of Cu(0 0 1)/diamond(0 0 1) > Cu(1 1 1)/diamond(1 1 1) > Cu(0 1 1)/diamond(0 1 1). For Cu/Ni/diamond, the sequence changes to Cu(0 0 1)/Ni/diamond(0 0 1) > Cu(0 1 1)/Ni/diamond(0 1 1) > Cu(1 1 1)/Ni/diamond(1 1 1) for the interface between Cu and Ni-diamond while the interface stability between Cu–Ni and diamond keeps the same order with Cu/diamond. For Cu/N/diamond, Interf.I (between Cu and N-diamond) and Interf.II (between Cu–N and diamond) stabilities follow the same sequence with the unmodified Cu/diamond, where Cu(0 0 1)/N/diamond(0 0 1) is the most stable, followed by Cu(1 1 1)/N/diamond(1 1 1).

The metallic interfacial additive Ni is found to enhance the Cu(0 1 1)/diamond(0 1 1) interfacial stability. Note that bulk Cu and diamond are both face-centered cubic structured exposing the most stable surface (1 1 1), and interestingly, the nonmetallic element N, exhibiting a quasi-bulk-CuCN structure with its bonded Cu and N at the interface forming the eutectic interfacial boundary, is found to promote the stability of Cu(1 1 1)/diamond(1 1 1) where the work of adhesion W_{ad} of Interf.I and Interf.II are both larger than the unmodified one.

In addition to the type of formed interfacial boundary, subsequent calculations of electronic properties show that the stability of the interface is also related to the interfacial bond populations and bond numbers. The LPDOS, charge density and charge density difference maps, and bond populations analyses all reveal that in addition to the 4s, the 4p and 3d orbitals of interfacial Cu are also involved in the orbitals hybridization. The atomic charges analyses reveal that the interfacial Ni additive acts as an electron donor contributing the electrons to its bonded Cu and C atoms while interfacial N atom is an electron acceptor accepting the electrons from its bonded Cu and C. The charge density map together with the work of adhesion suggests that the formed interfacial bond strength decreases in the order of covalent C–N > ionic C–Ni > ionic C–Cu.

ORCID iDs

Xue-Rong Shi ⓘ https://orcid.org/0000-0001-7455-8363

References

[1] Rosinski M, Ciupinski L, Grzonka J, Michalski A and Kurzydlowski K J 2012 Synthesis and characterization of the diamond/copper composites produced by the pulse plasma sintering (PPS) method *Diam. Relat. Mater.* **27–8** 29–35

[2] Aldwell B, Yin S, McDonnell K A, Trimble D, Hussain T and Lupoi R 2016 A novel method for metal–diamond composite coating deposition with cold spray and formation mechanism *Scr. Mater.* **115** 10–3

[3] Lu C, Tian Y, Shen Y, Feng X and Jiang J 2018 Thermal shock resistance and thermal conductivity of diamond-Cu composite coatings on Cu substrate via mechanical milling method *Surf. Coat. Technol.* **352** 529–40

[4] Bai G, Wang L, Zhang Y, Wang X, Wang J, Kim M J and Zhang H 2019 Tailoring interface structure and enhancing thermal conductivity of Cu/diamond composites by alloying boron to the Cu matrix *Mater. Charact.* **152** 265–75

[5] Chen L, Chen S and Hou Y 2019 Understanding the thermal conductivity of Diamond/Copper composites by first-principles calculations *Carbon* **148** 249–57

[6] Dong Y, Zhang R, He X, Ye Z and Qu X 2012 Fabrication and infiltration kinetics analysis of Ti-coated diamond/copper composites with near-net-shape by pressureless infiltration *Mater. Sci. Eng.* B **177** 1524–30

[7] Jhong Y-S, Hsieh M-C and Lin S-J 2019 Effect of Ag/Cu matrix composition on thermal properties of diamond/Ag/Cu-Ti composites fabricated by pressureless sintering *Mater. Lett.* **254** 316–9

[8] Yang L, Sun L, Bai W and Li L 2019 Thermal conductivity of Cu-Ti/diamond composites via spark plasma sintering *Diam. Relat. Mater.* **94** 37–42

[9] Zhang Y, Zhang H L, Wu J H and Wang X T 2011 Enhanced thermal conductivity in copper matrix composites reinforced with titanium-coated diamond particles *Scr. Mater.* **65** 1097–100

[10] Lin B, Wang X, Zhang Y, Zhu J and Zhang H 2015 Interface characterization of a Cu–Ti-coated diamond system *Surf. Coat. Technol.* **278** 163–70

[11] Schubert T, Ciupiński Ł, Zieliński W, Michalski A, Weißgärber T and Kieback B 2008 Interfacial characterization of Cu/diamond composites prepared by powder metallurgy for heat sink applications *Scr. Mater.* **58** 263–6

[12] Kang Q, He X, Ren S, Zhang L, Wu M, Guo C, Cui W and Qu X 2013 Preparation of copper–diamond composites with chromium carbide coatings on diamond particles for heat sink applications *Appl. Therm. Eng.* **60** 423–9

[13] Ciupiński Ł, Kruszewski M J, Grzonka J, Chmielewski M, Zielińsk R, Moszczyńska D and Michalski A 2017 Design of interfacial Cr_3C_2 carbide layer via optimization of sintering parameters used to fabricate copper/diamond composites for thermal management applications *Mater. Des.* **120** 170–85

[14] Lu C, Feng X, Shen Y, Tian Y, Jiang J and Hu L 2019 Wear resistance and thermal conductivity of diamond/ Cu-1Cr mechanical milled coatings after high temperature annealing *Diam. Relat. Mater.* **97** 107438

[15] Gu K, Pang M and Zhan Y 2019 Insight into interfacial structure and bonding nature of diamond(0 0 1)/Cr_3C_2(0 0 1) interface *J. Alloys Compd.* **770** 82–9

[16] Liu Z, Zheng S, Lu Z, Pu J and Zhang G 2018 Adhesive transfer at copper/diamond interface and adhesion reduction mechanism with fluorine passivation: a first-principles study *Carbon* **127** 548–56

[17] Wang J, Wang F, Li J, Sun Q, Yuan P and Jia Y 2013 Comparative study of friction properties for hydrogen- and fluorine-modified diamond surfaces: a first-principles investigation *Surf. Sci.* **608** 74–9

[18] Erdemir A 2001 The role of hydrogen in tribological properties of diamond-like carbon films *Surf. Coat. Technol.* **146–7** 292–7

[19] Schäfer D, Eisenmenger-Sittner C, Chirtoc M, Kijamnajsuk P, Kornfeind N, Hutter H, Neubauer E and Kitzmantel M 2011 Characterization of the mechanical and thermal interface of copper films on carbon substrates modified by boron based interlayers *Surf. Coat. Technol.* **205** 3729–35

[20] Hell J, Chirtoc M, Eisenmenger-Sittner C, Hutter H, Kornfeind N, Kijamnajsuk P, Kitzmantel M, Neubauer E and Zellhofer K 2012 Characterisation of sputter deposited niobium and boron interlayer in the copper–diamond system *Surf. Coat. Technol.* **208** 24–31

[21] Bai Z, Chen X, Yang K, Guan W, Li C, Chen P and Liang C 2019 Hydrogenation of dicyclopentadiene resin and its monomer over high efficient CuNi alloy catalysts *ChemistrySelect* **4** 6035–42

[22] Wang W, Wang Y, Liu S, Yahia M, Dong Y and Lei Z 2019 Carbon-supported phosphatized CuNi nanoparticle catalysts for hydrazine electrooxidation *Int. J. Hydrog. Energy* **44** 10637–45

[23] Zhang R, Guo X, Wang B and Ling L 2015 Insight into the effect of CuNi(1 1 1) and FeNi(1 1 1) surface structure and second metal composition on surface carbon elimination by O or OH: a comparison study with Ni(1 1 1) surface *J. Phys. Chem.* C **119** 14135–44

[24] Syugaev A V, Lyalina N V, Lomayeva S F and Maratkanova A N 2016 The electrochemical properties of Ni_3C carbide *J. Solid State Electrochem.* **20** 775–84

[25] Gibson J S, Uddin J, Cundari T R, Bodiford N K and Wilson A K 2010 First-principle study of structure and stability of nickel carbides *J. Phys.: Condens. Matter* **22** 445503

[26] Liu X, Dronskowski R, Kremer R K, Ahrens M, Lee C and Whangbo M-H 2008 Characterization of the magnetic and structural properties of copper carbodiimide, CuNCN, by neutron diffraction and first-principles evaluations of its spin exchange interactions *J. Phys. Chem.* C **112** 11013–7

[27] Hibble S J, Cheyne S M, Hannon A C and Eversfield S G 2002 CuCN: a polymorphic material. Structure of one form determined from total neutron diffraction *Inorg. Chem.* **41** 4990–2

[28] Deng J, Zhang J, Tu Y, Yang P, An M and Wang P 2018 Effect of BEO in the electrodeposition process of Ni/diamond composite coatings for preparation of ultra-thin dicing blades: experiments and theoretical calculations *Ceram. Int.* **44** 16828–36

[29] Wang X, Wang C, Shen X, Larsson K and Sun F 2019 DFT calculations of energetic stability and geometry of O-terminated B- and N-doped diamond (1 1 1)-1 × 1 surfaces *J. Phys.: Condens. Matter* **31** 265002

[30] Zhao D, Gao W, Li Y, Zhang Y and Yin H 2019 The electronic properties and band-gap discontinuities at the cubic boron nitride/diamond hetero-interface *RSC Adv.* **9** 8435–43

[31] Dürrbeck S, Shi X-R, Samadashvili M, Redinger J, Bertel E and Salmeron M 2018 Complex reactions on a convertible catalyst surface: a study of the S–O–Cu system *Surf. Sci.* **678** 228–33

[32] Pang X, Yang J, Pang M, He J, Yang W, Qin H and Zhan Y 2019 Theoretical understanding of atomic and electronic structures of the ZrC(1 1 1)/Cu(1 1 1) interface *J. Alloys Compd.* **791** 431–7

[33] Vanderbilt D 1990 Soft self-consistent pseudopotentials in a generalized eigenvalue formalism *Phys. Rev.* B **41** 7892–5

[34] Perdew J P, Burke K and Ernzerhof M 1996 Generalized gradient approximation made simple *Phys. Rev. Lett.* **77** 3865–8

[35] Clark S J, Segall M D, Pickard C J, Hasnip P J, Probert M I J, Refson K and Payne M C 2005 First principles methods using CASTEP *Z. Kristallogr.* **220** 567–70

[36] Siegel D J, Hector L G and Adams J B 2002 First-principles study of metal–carbide/nitride adhesion: Al/VC versus Al/ VN *Acta Mater.* **50** 619–31

[37] Zhao W, Wang L, Yu Z, Chen J and Yang J 2019 A processing technology of grooves by picosecond ultrashort pulse laser in Ni alloy: enhancing efficiency and quality *Opt. Laser Technol.* **111** 214–21

[38] Lu N *et al* 2017 Yolk–shell nanostructured Fe_3O_4 @C magnetic nanoparticles with enhanced peroxidase-like activity for label-free colorimetric detection of H_2O_2 and glucose *Nanoscale* **9** 4508–15

[39] Zhang R, Lu N, Zhang J, Yan R, Li J, Wang L, Wang N, Lv M and Zhang M 2020 Ultrasensitive aptamer-based protein assays based on one-dimensional core–shell nanozymes *Biosens. Bioelectron.* **150** 111881

[40] Stampfl C, Derry T E and Makau N W 2010 Interaction of diamond(1 1 1)—(1 × 1) and (2 × 1) surfaces with OH: a first principles study *J. Phys.: Condens. Matter* **22** 475005

[41] Tiwari A K, Goss J P, Briddon P R, Wright N G, Horsfall A B and Rayson M J 2012 Electronic and structural properties of diamond (0 0 1) surfaces terminated by selected transition metals *Phys. Rev.* B **86** 155301